Electronic Supplementary Material (ESI) for Journal of Materials Chemistry A.

Electronic Supplementary Information

Sol-gel asynchronous crystallization of ultra-selective metal-organic framework membranes for gas separation

Wanbin Li,* Wufeng Wu, Zhanjun Li, Jiali Shi and Yan Xia

School of Environment, Guangzhou Key Laboratory of Environmental Exposure and Health, and Guangdong Key Laboratory of Environmental Pollution and Health, Jinan University, Guangzhou 511443, P.R. China.

E-mail: gandeylin@126.com

Experimental

Gel Fabrication

Zinc acetate dihydrate (5.2 g) was added into ethanol (15.0 ml) and stirred at 60 °C to obtain the white suspension. Ethanolamine (1.5 ml) was dropped into the suspension under stirring at 60 °C to fabricate the transparent sol. For achieving the precursor gel, 2-methylimidazole (MeIM) was dispersed into the prepared sol with stirring. The amount of MeIM was changed to prepare the gels with various MeIM/Zn ratios. After violent stirring, the white gel was formed.

ZIF-8 Membrane Fabrication

Anodic aluminum oxide (AAO) substrate with diameter 25 mm and pore size of 20 nm was employed for supporting the ZIF-8 membranes. The substrate was fixed on a coater by suction for spin-coating. To prevent the direct suction of vacuum pump towards the coating gel, AAO substrate was stacked on an impermeable cushion. The prepared gel with volume of 200 μl was coated on AAO substrate at rotation rate of 6000 rpm. For membrane formation, the gel film was thermally treated with temperature of 120 °C for 40 h. After crystallization, the prepared membrane was washed by methanol and dried at room temperature for several days.

For synthesizing the ultrathin ZIF-8 membrane, the sol was diluted to the certain concentration and MeIM with corresponding amount was added under violent stirring to achieve the diluted gel. Subsequently, the gel was coated on AAO substrate and thermally treated for preparing the ultrathin ZIF-8 membrane.

For preparation of the ZIF-8 hollow fiber membrane, polyvinylidene fluoride (PVDF) hollow fiber was fabricated and ammoniated by ethanediamine to improve the chemical stability. In typical process, PVDF hollow fiber was immersed in ethanediamine solution with concentration of 25 v/v% and heat-treated at 150 ^oC for 20 h. After reaction, the ammoniated hollow fiber was rinsed by ethanol and water for several times, and dried at room temperature for use. The modified PVDF hollow fiber was immersed in the gel and maintained for 20 seconds. After gel loading, the hollow fiber was taken out and purged by nitrogen. The loaded hollow fiber was vertically fixed on a homemade shelf and subjected to thermal-treatment for crystallization. Subsequently, the prepared membranes was washed and dried.

Characterization

X-ray diffraction (XRD) was employed to study the crystalline structure of the gels and ZIF-8 membranes. The patterns were recorded by X-ray diffractometer (D2 Phaser, Bruker CO.) at 30 kV and 10 mA. The samples were scanned using a step size of 0.01^o and a scan speed of 0.2 s per step. The data was recorded for 2θ angles between 5° and 40°.

A fourier transform infrared spectrophotometer with attenuated total reflectance mode (IRTracer-100, Shimadzu CO.) was used to characterize the change of the chemical structure of the prepared ZIF-8 membranes.

The morphology of the prepared membranes was observed by using a field-emission scanning electron microscope (Ultra-55, Zeiss Co.) with accelerating voltage of 5 kV. The attached X-ray energy dispersion spectroscopy was applied to investigate the element distribution of the prepared membranes. An ultrathin gold layer was coated on the prepared samples by using an ion sputter coater to minimize charging effects.

Transmission electron microscopy (TEM) images of the ZIF-8 colloidal crystals were collected by using a JEM-2100 (JEOL Co.) with accelerating voltage of 200 kV. For preparation of samples, gel (50 μl) was added in ethanol (5.0 ml) and then subjected to ultrasonic treatment for 30 min. The diluted gel was dropped on an ultrathin carbon film with copper net.

A physisorption analyzer (Autosorb iQ Station 1, Quantachrome Co.) was applied to study the porosity of the membranes. N_2 adsorption-desorption isotherms were measured at 77.35 K held using liquid nitrogen bath. Before measurement, the sample was treated in vacuum at 120 °C for 12 h. Multi-Point BET method was used to calculate the specific surface area with P/P_0 range from 0.003-0.05. Micropore area was obtained by V-t method with P/P_0 range from 0.2-0.35. Pore width was achieved by DFT method.

A RBD upgraded PHI-5000C ESCA system (Perkin Elmer) with an incident radiation of monochromatic Mg Kα X-rays (hν=1253.6 eV) at 250 W was employed to perform X-ray photoelectron spectroscopy (XPS) experiments. The high voltage was kept at 14.0 kV. To ensure sufficient resolution and sensitivity, the pass energy was set as 46.95 eV. In analysis chamber, the pressure was below 5×10^{-8} Pa. The spectra of all the elements were collected by using RBD 147 interface (RBD Enterprises, USA).

Single-component permeation of the membranes was investigated by constant-pressure, variable-volume method. The membrane with effective area of 3.14 cm^2 was sealed in a permeation cell by O-ring. For hollow fiber membrane, it was sealed in a permeation module by epoxy resins with effective area of 1.37 cm^2. The gas permeation experiment was carried out with different kinetic diameters (KD) of gases in the following order: H_2 (KD: 0.289 nm), CO_2 (KD:

0.33 nm), O_2 (KD: 0.346 nm), N_2 (KD: 0.364 nm), CH_4 (KD: 0.38 nm), C_3H_6 (KD: 0.40 nm), C_3H_8 (KD: 0.43 nm), C_3H_8, C_3H_6, CH_4, N_2, O_2, CO_2, and H_2. After running steadily, the data was read and recorded. Separation performance of H_2/CH_4, H_2/C_3H_8 and C_3H_6/C_3H_8 mixtures through the membranes was investigated by a converted mixed gas permeability analyzer. The equimolar feed mixture was fed to the sides of the dense layer of membranes with flow rate of 30 ml/min. The composition of the mixture was analyzed using gas chromatography. The reported data of single-component permeation and mixture separation were calculated by averaging the measured values of three membrane samples. The ideal selectivity is defined as the ratio of two kinds of single-component permeances. The selectivity of mixture separation, for example of H_2/CH_4 separation, is calculated via dividing the molar ratio (H_2 to CH_4) of the permeate gases by the molar ratio (H_2 to CH_4) of the retentate gases.

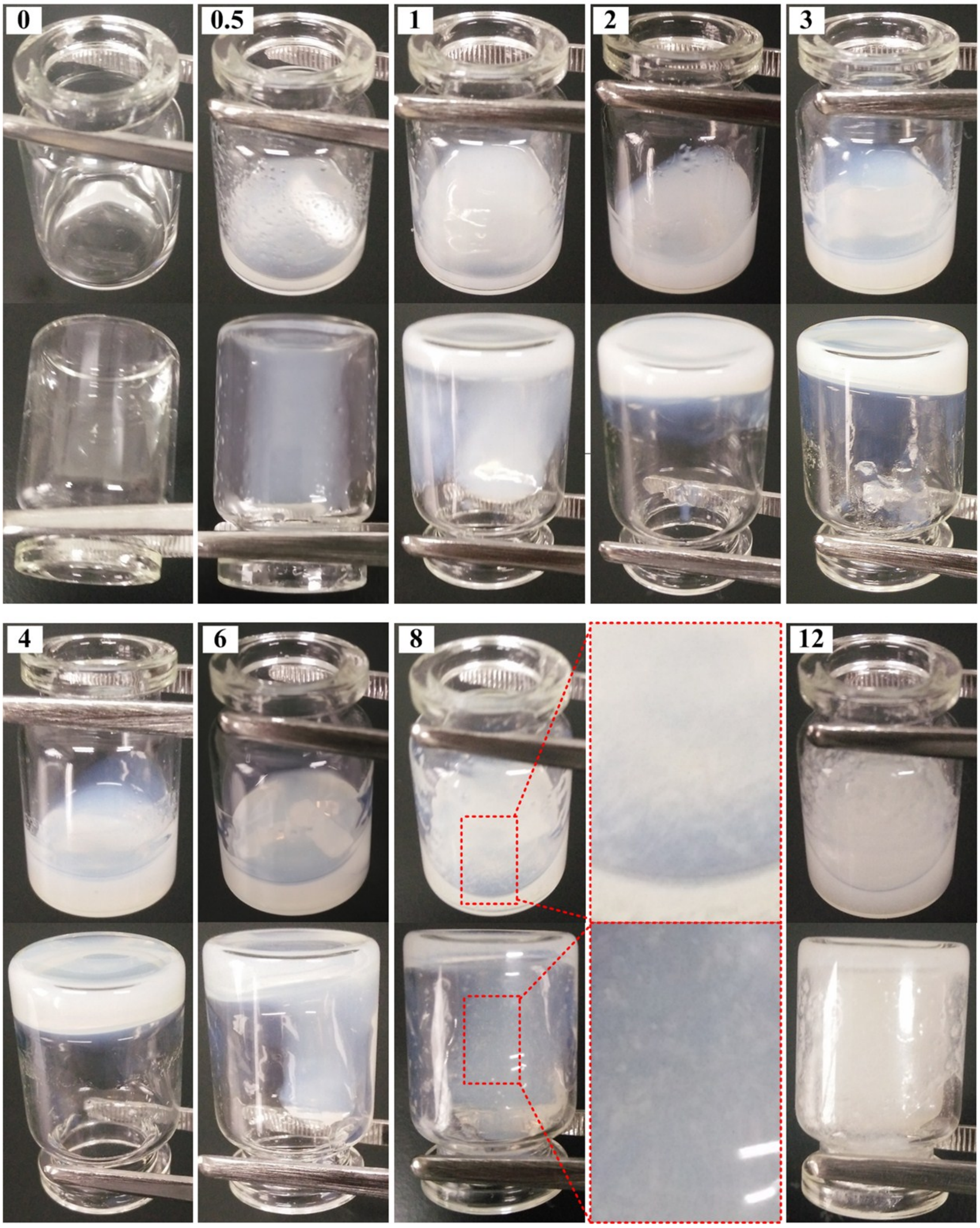

Fig. S1 The photographs of the gels with MeIM/Zn ratios of 0, 0.5, 1, 2, 3, 4, 6, 8 and 12. The flow of the gels with MeIM/Zn ratios of 0, 0.5, 1, 6, 8 and 12 demonstrated the relatively lower viscosity. The enlarged photographs of the gel with MeIM/Zn ratio of 8 display the white plaques of the undissolved MeIM.

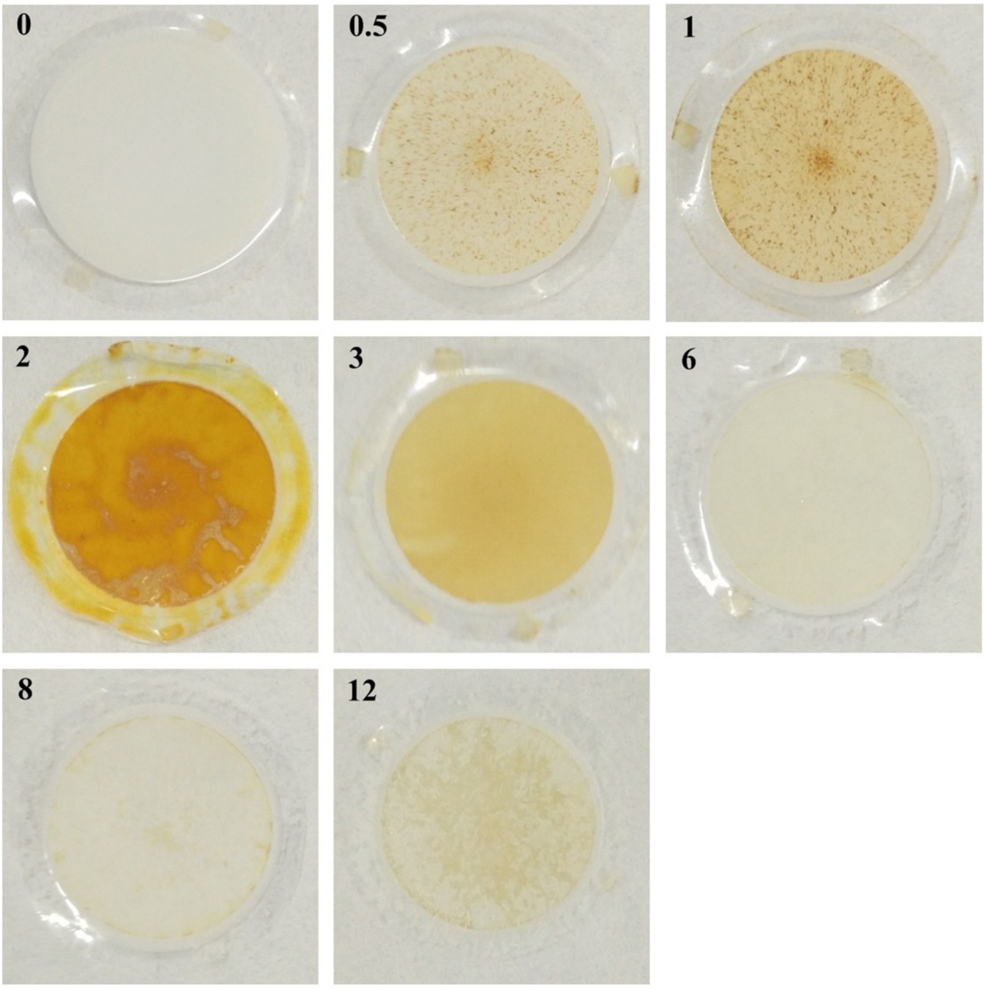

Fig. S2 The photographs of the ZIF-8 membranes prepared with MeIM/Zn ratios of 0, 0.5, 1, 2, 3, 6, 8 and 12.

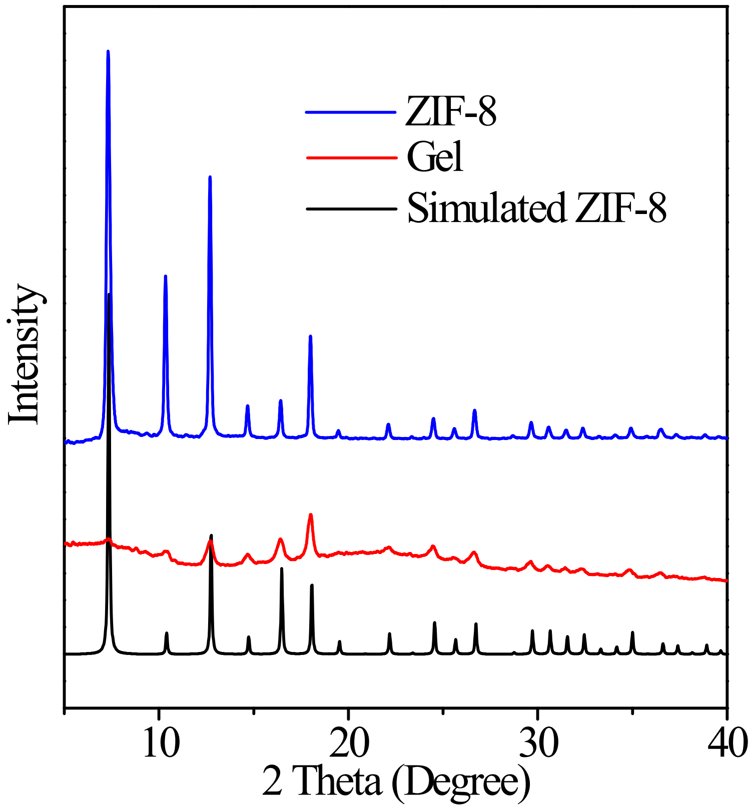

Fig. S3 XRD patterns of the gel and ZIF-8 membrane with MeIM/Zn ratio of 4. The simulated ZIF-8 pattern is presented for comparison.

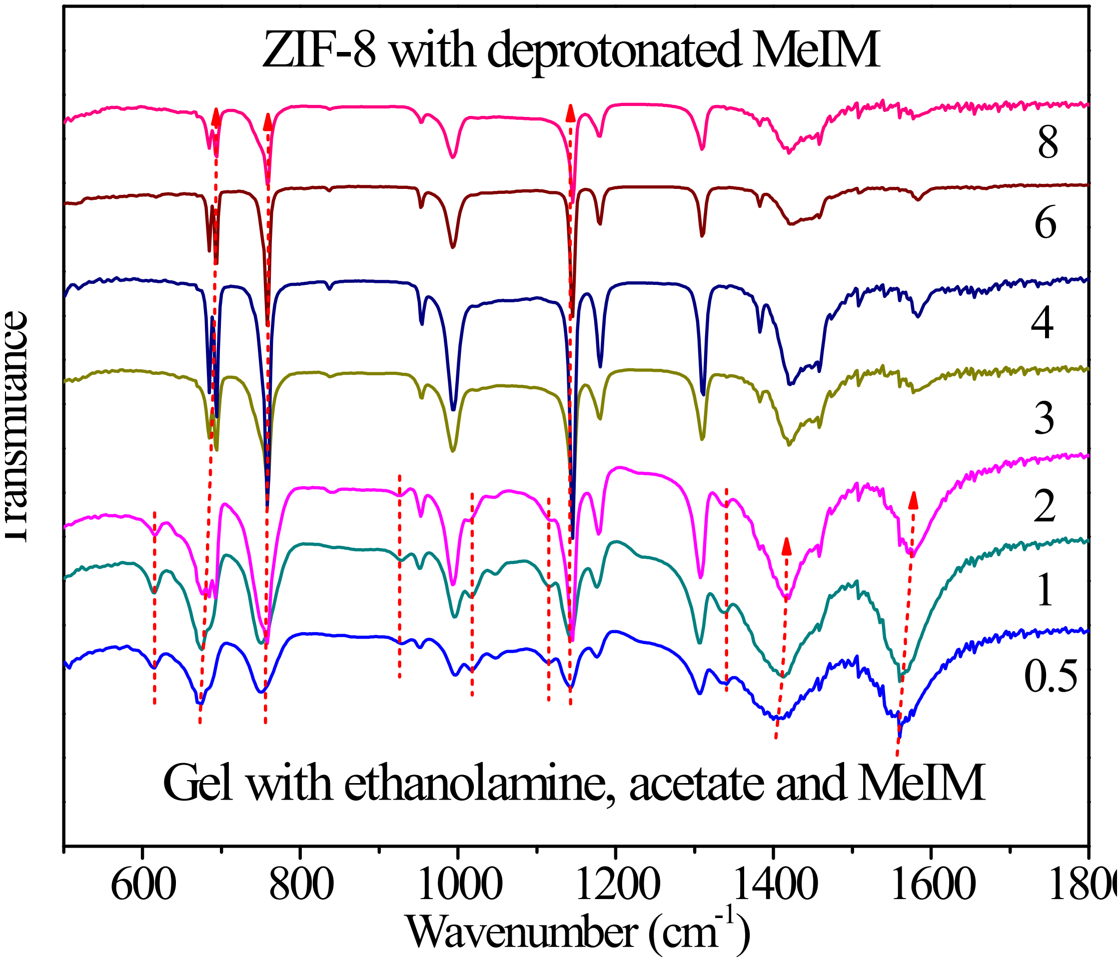

Fig. S4 FTIR spectra of the ZIF-8 membranes with various MeIM/Zn ratios. The changes of the characteristic peaks are marked by dotted lines. The change of the characteristic peaks were marked by red arrows.

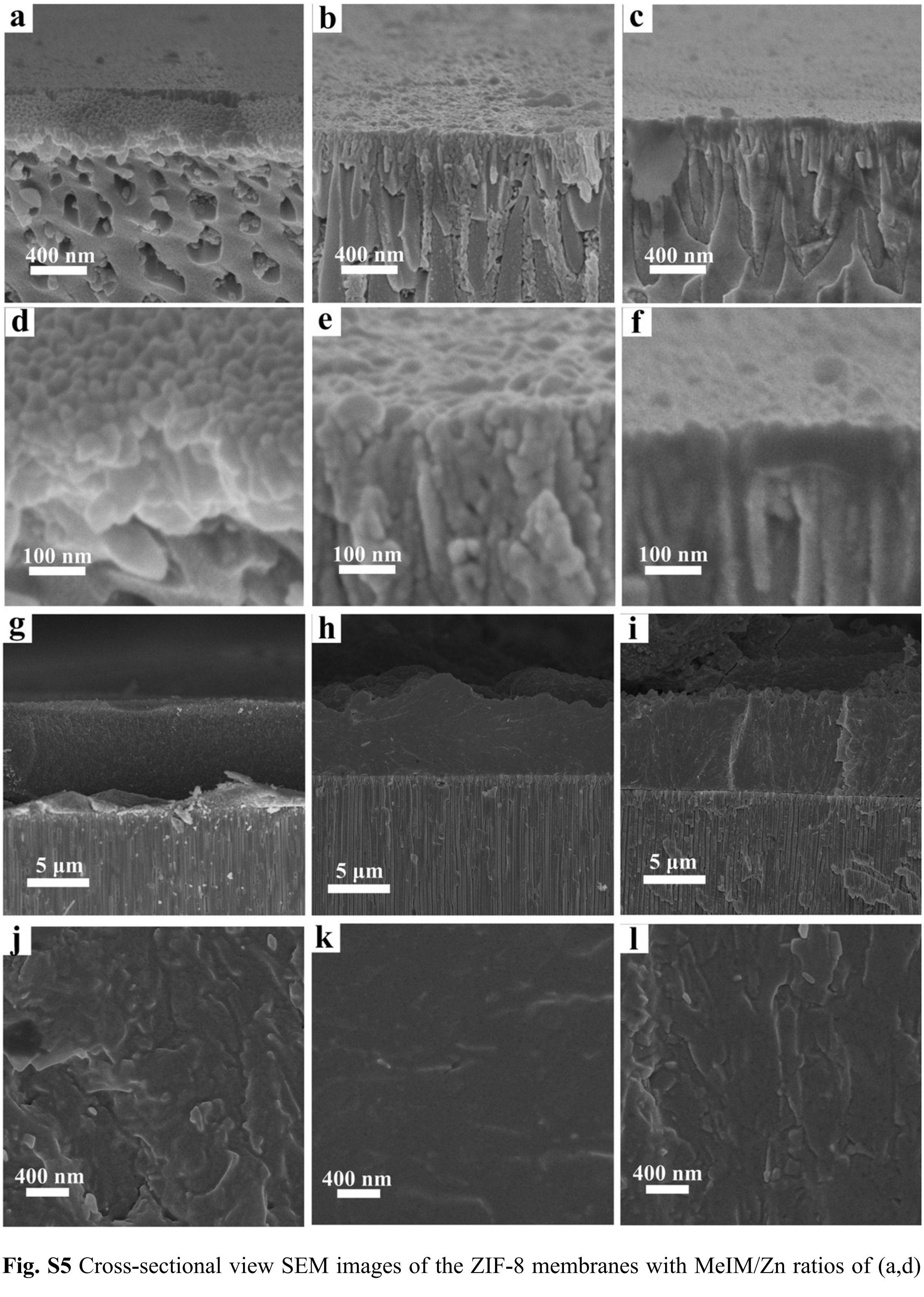

Fig. S5 Cross-sectional view SEM images of the ZIF-8 membranes with MeIM/Zn ratios of (a,d) 0, (b,e) 0.5, (c,f) 1, (g,j) 6, (h,k) 8 and (i,l) 12. The small thickness of the membranes with MeIM/Zn ratios of 0, 0.5 and 1 indicated the low gel loading.

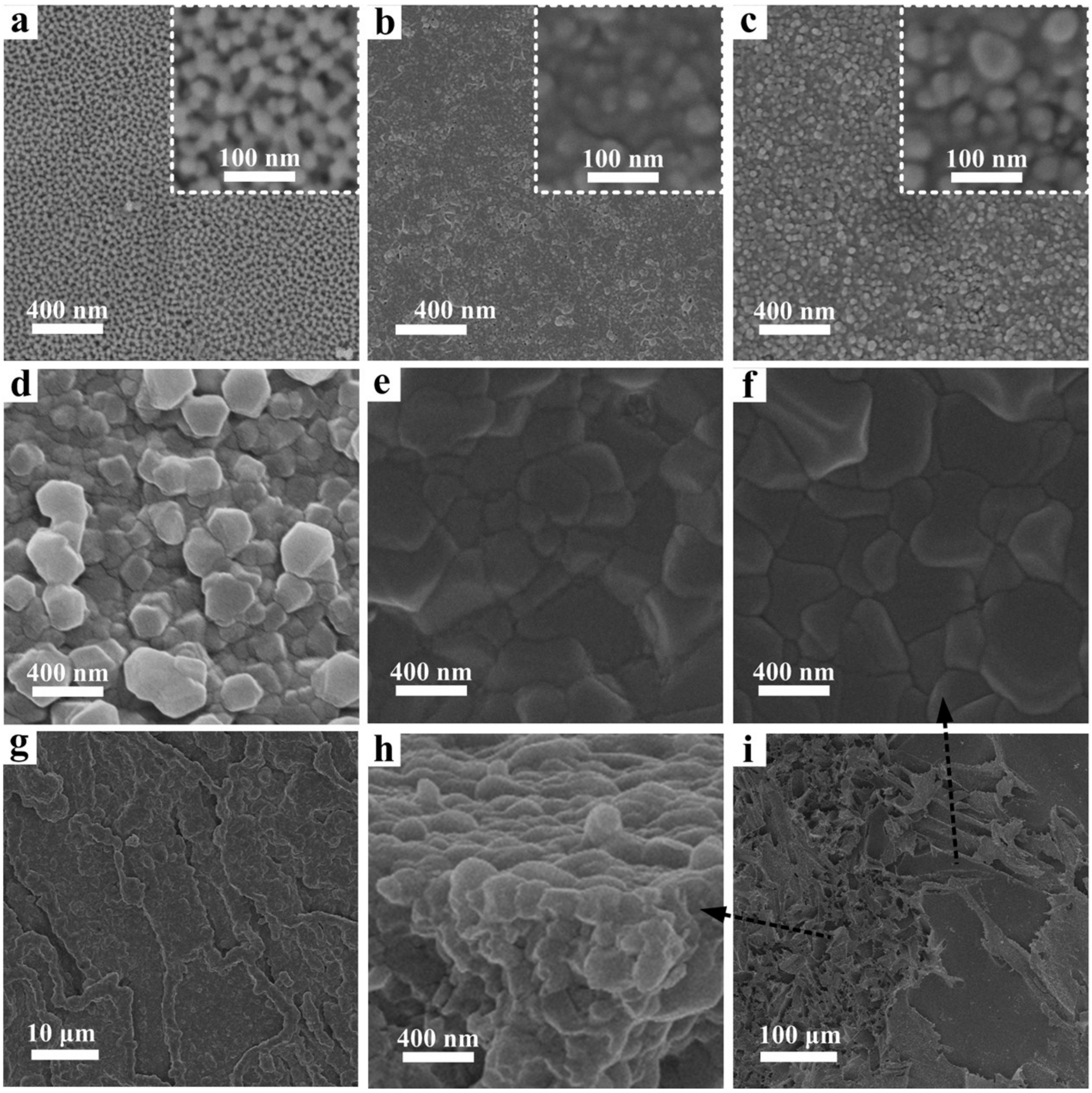

Fig. S6 Top view SEM images of the ZIF-8 membranes with MeIM/Zn ratios of (a) 0, (b) 0.5, (c) 1, (d) 6, (e,g) 8, and (f,h,i) 12. The rough morphologies shown in (g) and (i), and the (f,h) different structures at different regions of the membrane with MeIM/Zn ratio of 12 were resulted from the existence of the undissolved MeIM.

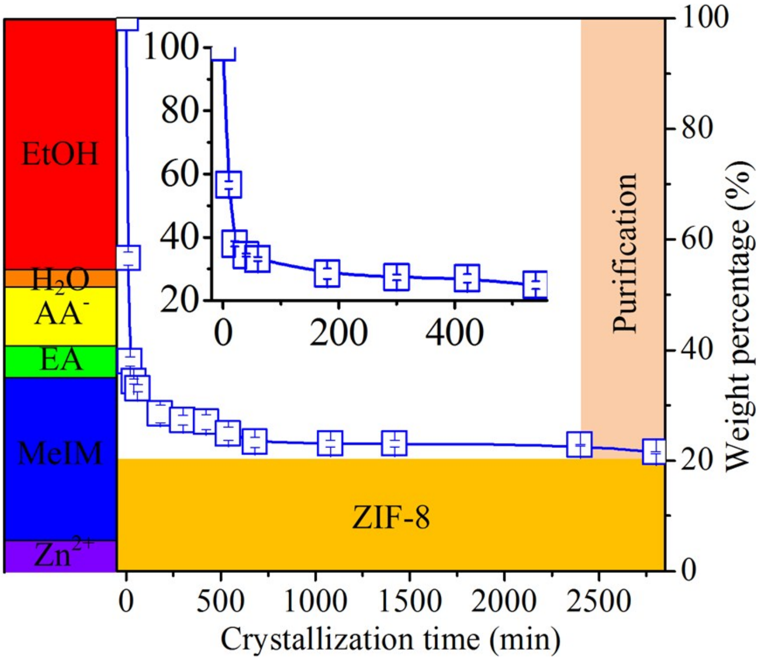

Fig. S7 The content of ethonal (EtOH), H_2O, acetate (AA^-), ethanolamine (EA), MeIM and zinc cation in original gel with MeIM/Zn ratio of 4, and the weight loss of ZIF-8 membrane formation process. The theoretical value of 20.4 % calculated by combination of zinc content in original gel and Zn ratio of ZIF-8 are presented for comparasion.

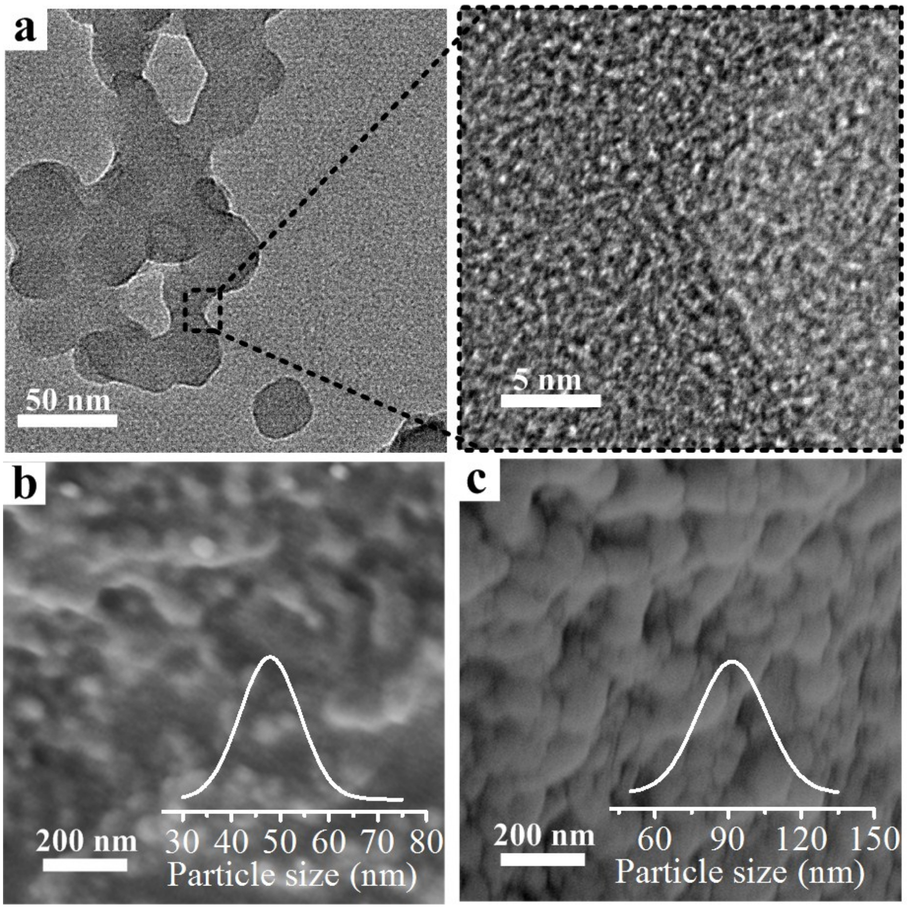

Fig. S8 (a) TEM images of the ZIF-8 nanocrystals in gel with MeIM/Zn ratio of 4. Cross-sectional view SEM images and particle size distributions of the ZIF-8 membranes with thermal-treatment for (b) 1 and (c) 3 h.

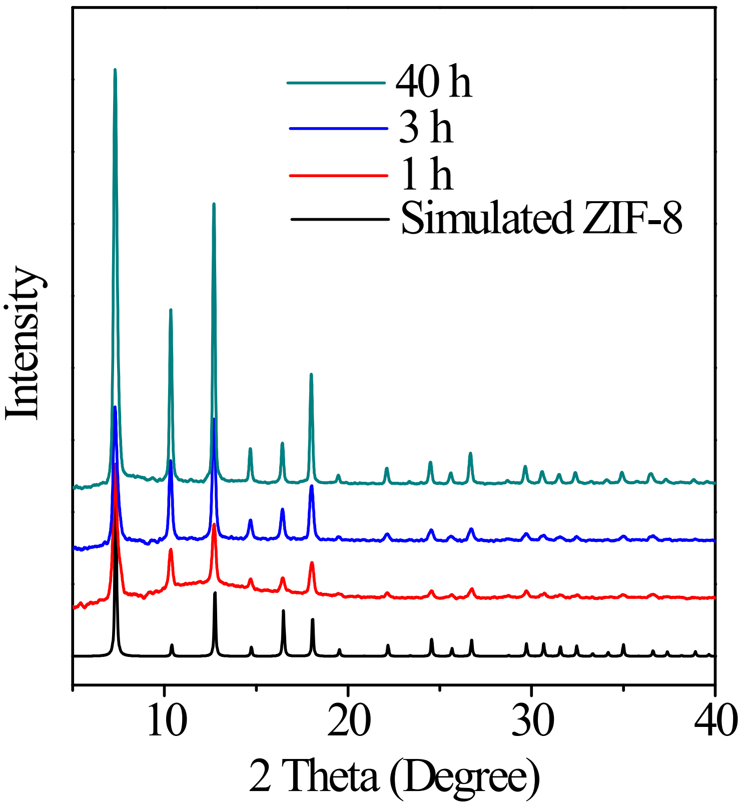

Fig. S9 XRD patterns of the ZIF-8 membranes with different thermal-treatment durations. With the extension of treatment time, the intensity of the characteristic peaks of ZIF-8 enhanced, demonstrating the proceeding of crystallization. The membranes were prepared with MeIM/Zn ratio of 4.

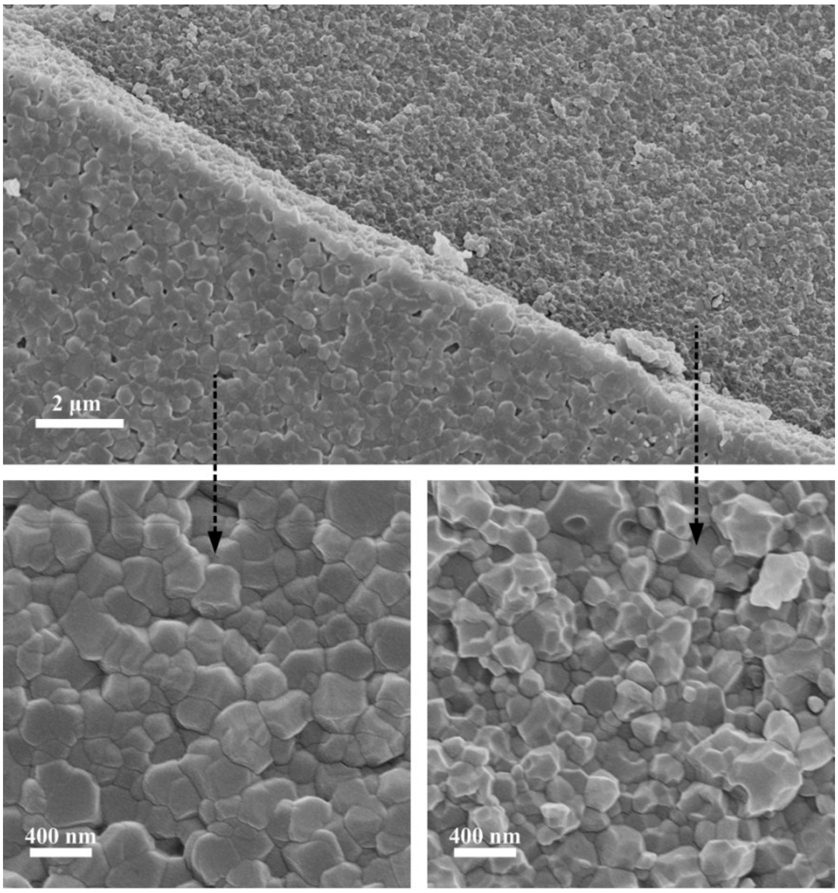

Fig. S10 SEM images of the surface and bottom fracture of the ZIF-8 membrane with MeIM/Zn ratio of 3.

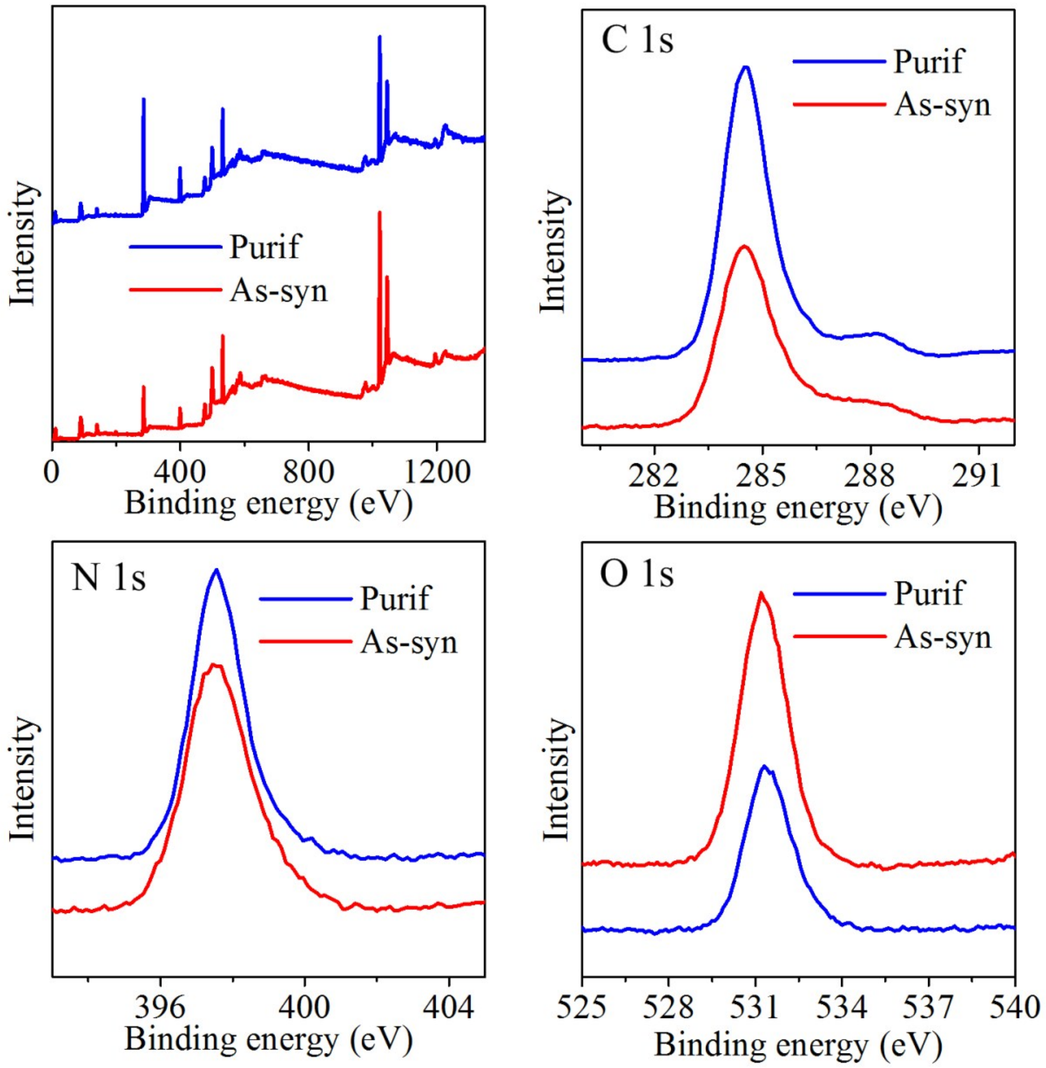

Fig. S11 XPS spectra of the as-synthesized and purified ZIF-8 membranes. Purification was performed by washing in methanol. The membranes were prepared with MeIM/Zn ratio of 4.

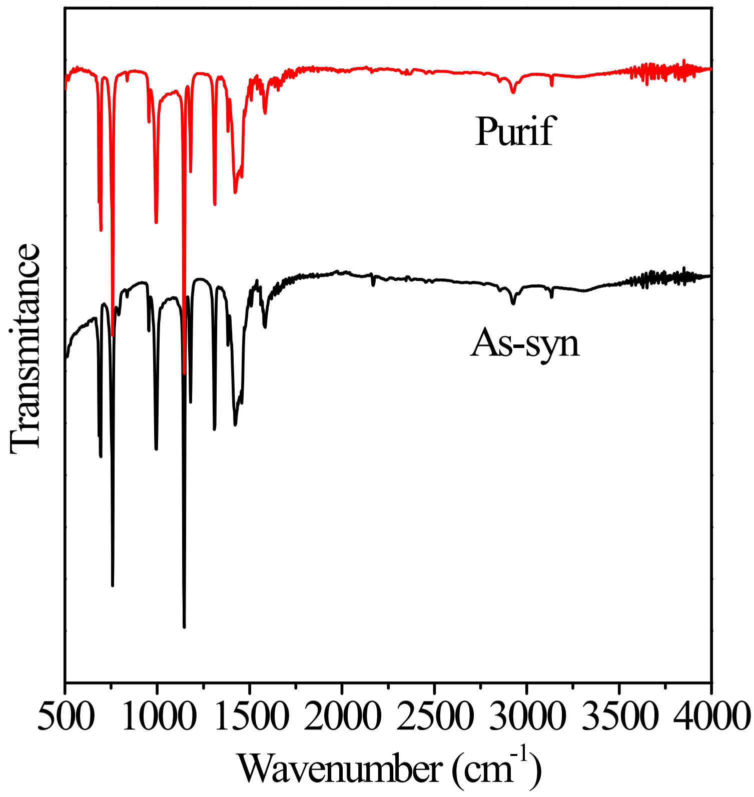

Fig. S12 FTIR spectra of the as-synthesized and purified ZIF-8 membranes. Purification was performed by washing in methanol. Because there were on difference in chemical structure of the primary materials, FTIR results showed hardly any change in spectra.

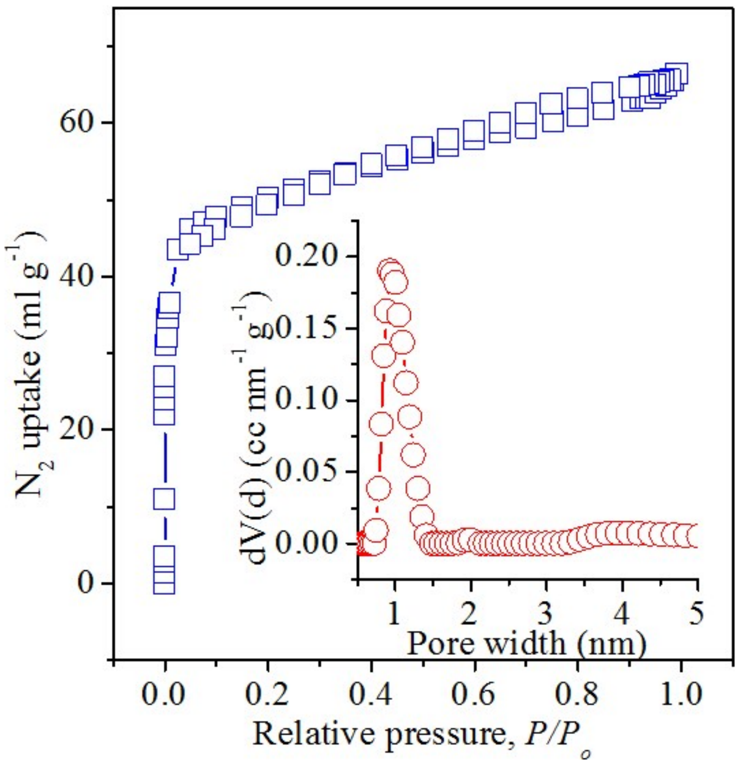

Fig. S13 N_2 adsorption-desorption isotherms and pore width distribution of the ZIF-8 membranes.

The membrane was prepared with MeIM/Zn ratio of 4. Pore width was calculated by DFT method.

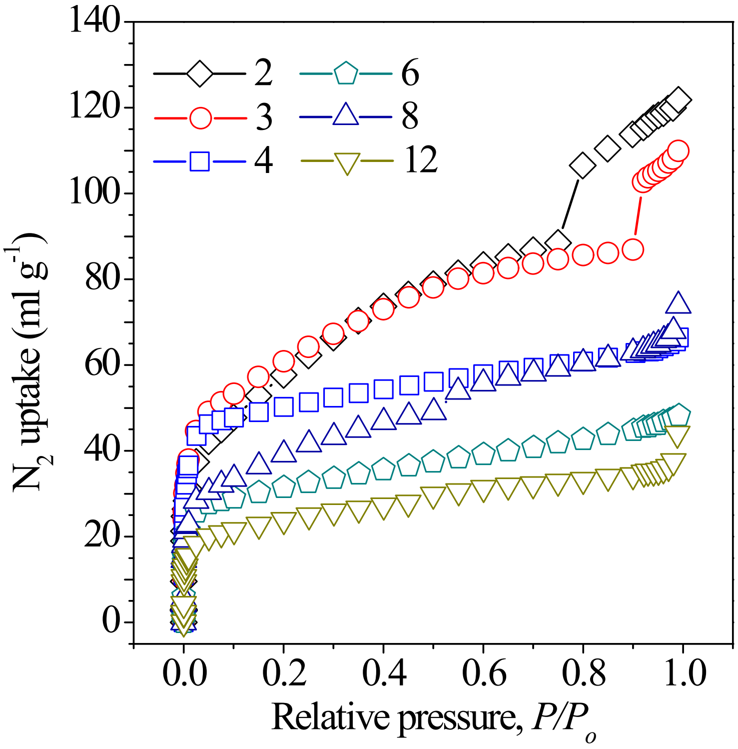

Fig. S14 N_2 adsorption isotherms of the ZIF-8 membranes with MeIM/Zn ratios from 2 to 12.

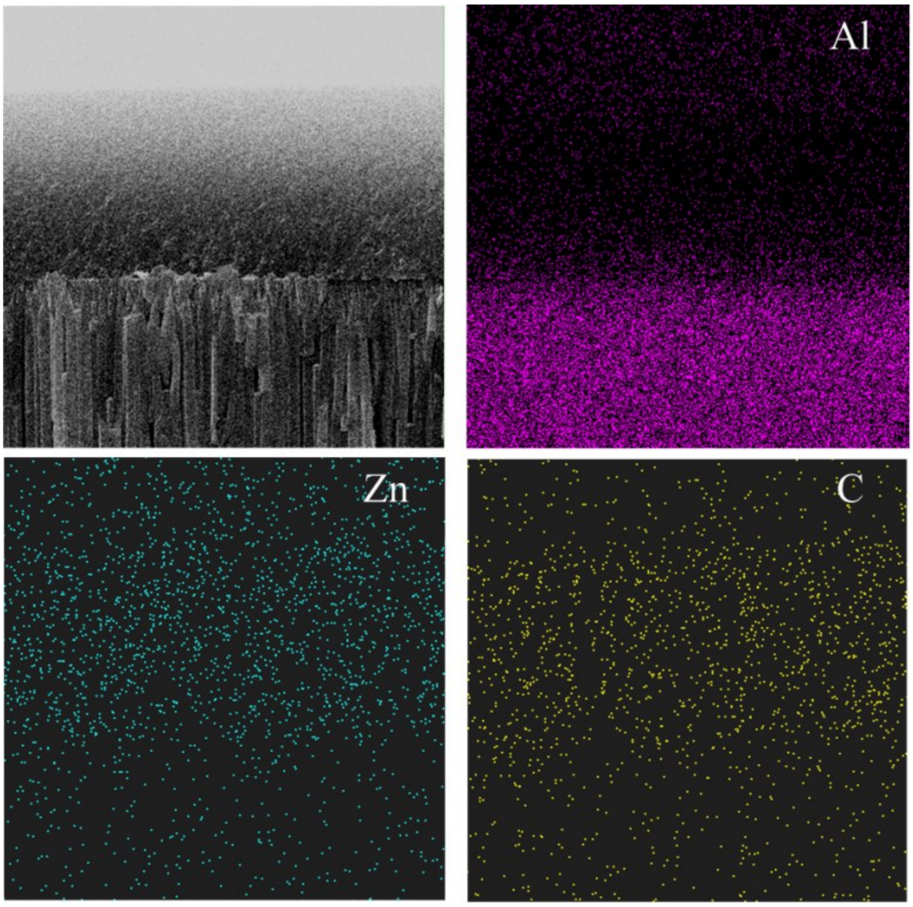

Fig. S15 Energy-dispersive x-ray mapping. The ZIF-8 membrane was prepared with MeIM/Zn ratio of 4.

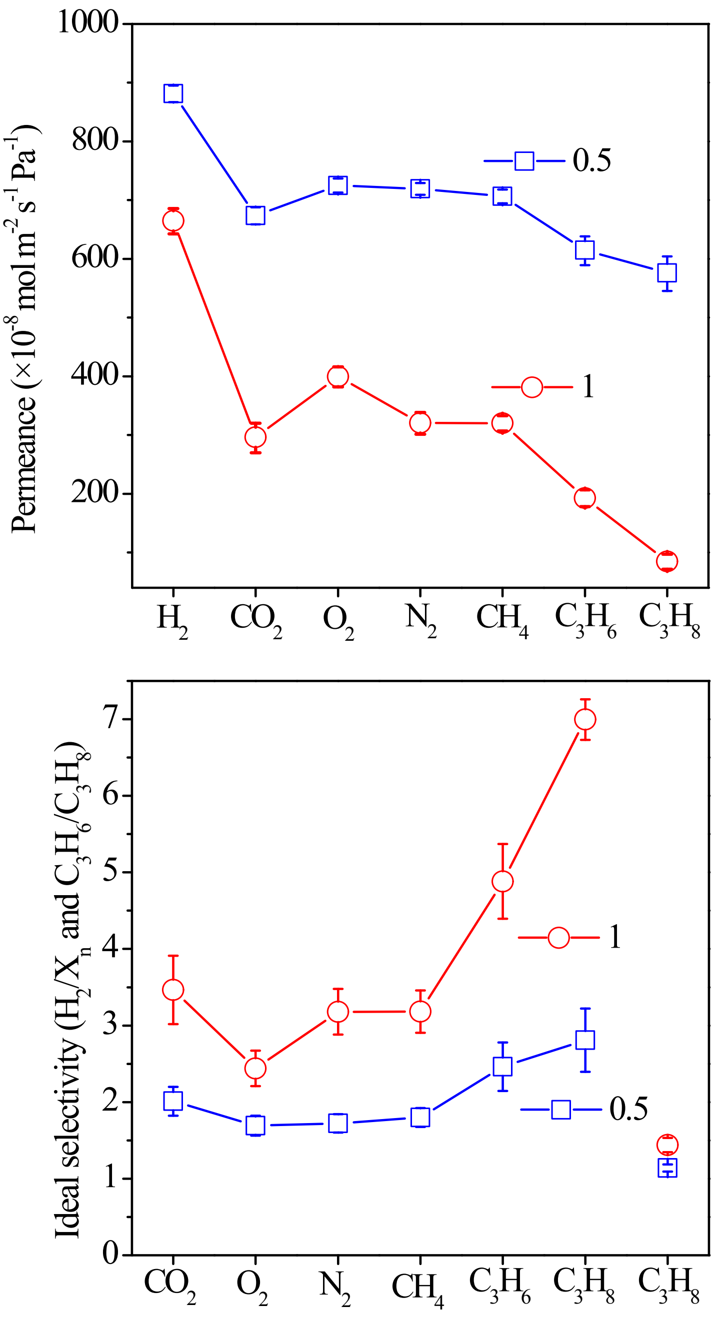

Fig. S16 Single-component permeances and ideal selectivities of the ZIF-8 membranes with MeIM/Zn ratios of 0.5 and 1. These membranes showed large permeances but small selectivities owing to the thin thickness and granular structure.

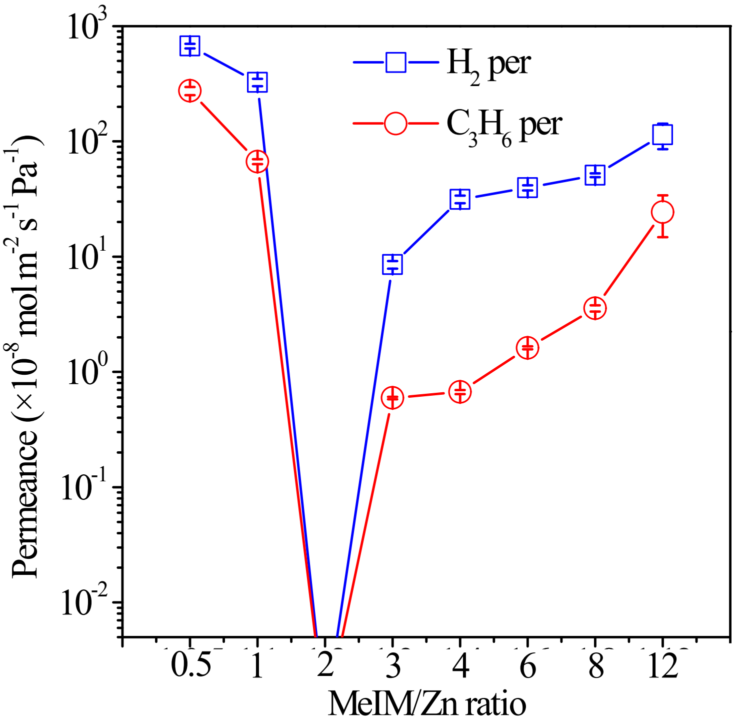

Fig. S17 Single-component permeances of H_2 and C_3H_6 through the ZIF-8 membranes with MeIM/Zn ratios from 0.5 to 12. The gas permeances displayed a downward and then upward tendency due to the change of membrane composition as the increased MeIM/Zn ratio.

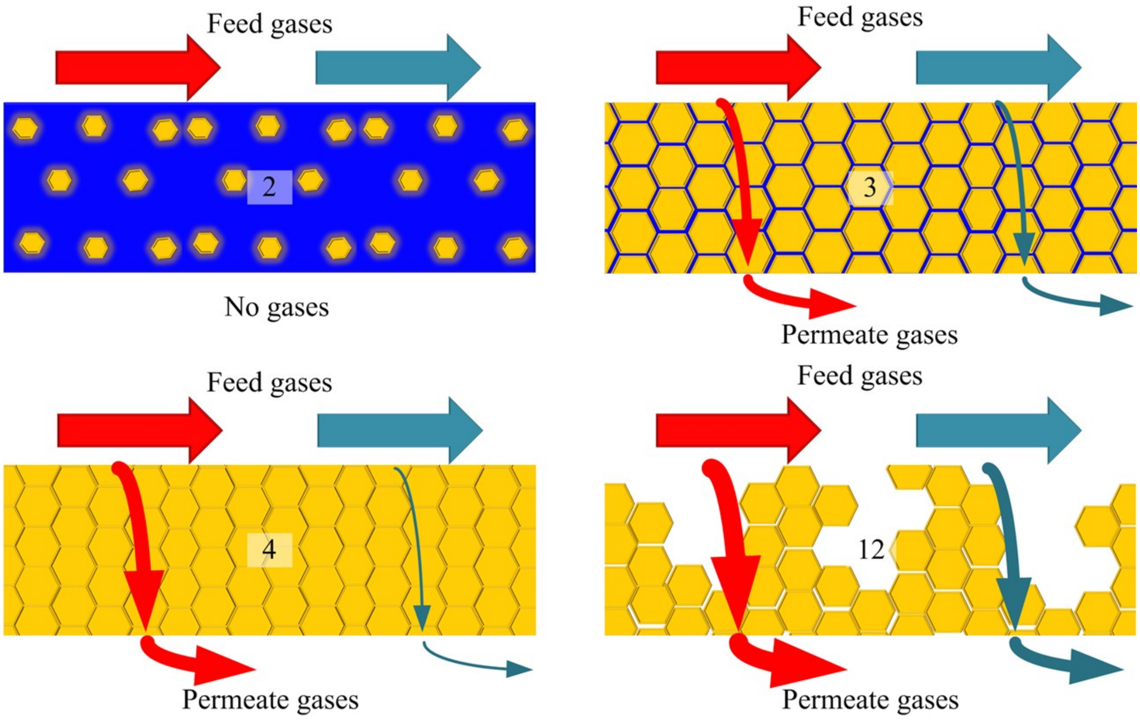

Fig. S18 Schematic of the gas separation through ZIF-8 membranes with various with MeIM/Zn ratios. The zinc complexes and ZIF-8 are depicted in blue and yellow.

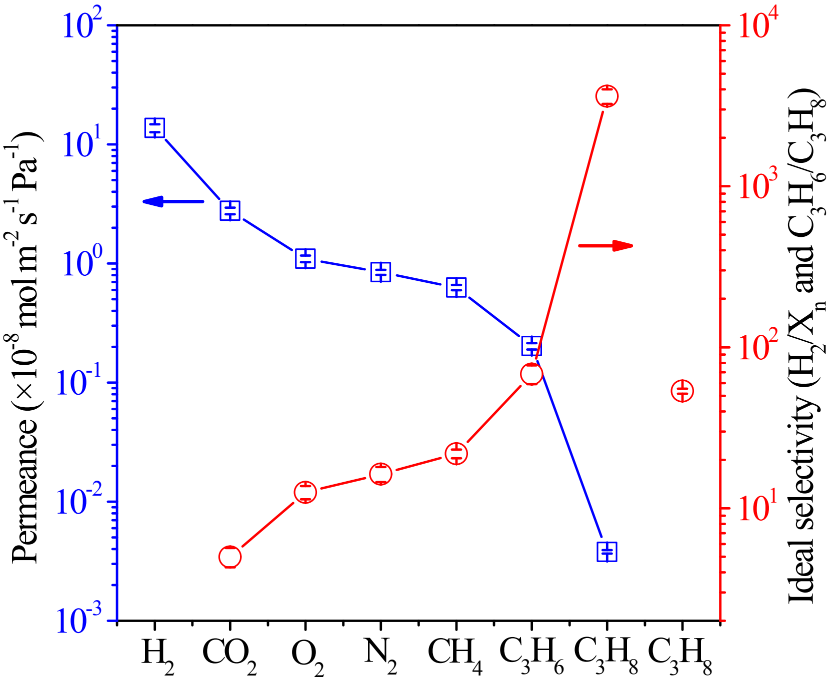

Fig. S19 Single-component permeances and ideal selectivities of the as-synthesized ZIF-8 membranes. The membrane was prepared with MeIM/Zn ratio of 4. Compared with the purified membrane, the as-synthesized membrane showed smaller permeances and relatively lower ideal selectivities due to the rarely residual zinc complexes.

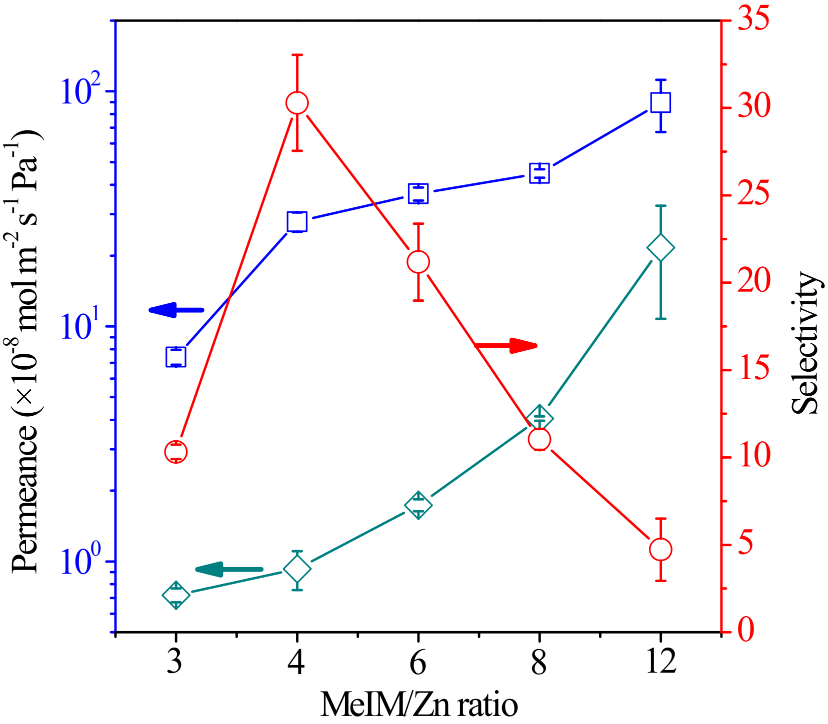

Fig. S20 Separation performance of the ZIF-8 membranes with various MeIM/Zn ratios for H_2/CH_4 mixture. Both H_2 and CH_4 permeances increased with increasing of MeIM/Zn ratio. Because of the variation in increase rate, H_2/CH_4 selectivity increased firstly and decreased subsequently. The membrane with MeIM/Zn ratio of 4 exhibited largest selectivity of 30.3 among the tested membranes.

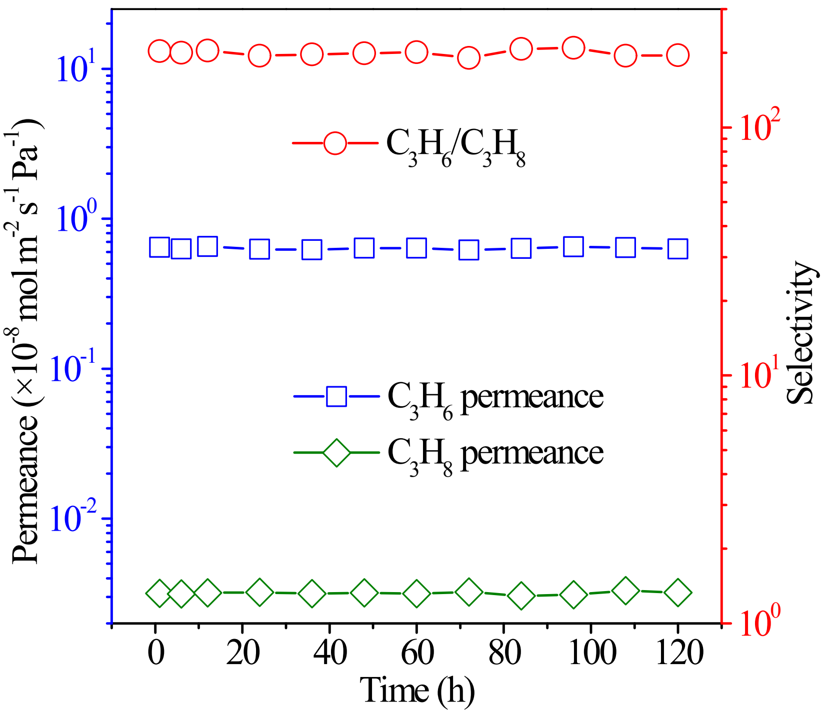

Fig. S21 Separation performance of the ZIF-8 membranes for C_3H_6/C_3H_8 mixture as a function of operation time. The small fluctuations of C_3H_6 permance, C_3H_8 permeance and C_3H_6/C_3H_8 selectivity over 5 days demonstrated the excellent long-term stability of the ZIF-8 membrane. The membrane was prepared with MeIM/Zn ratio of 4.

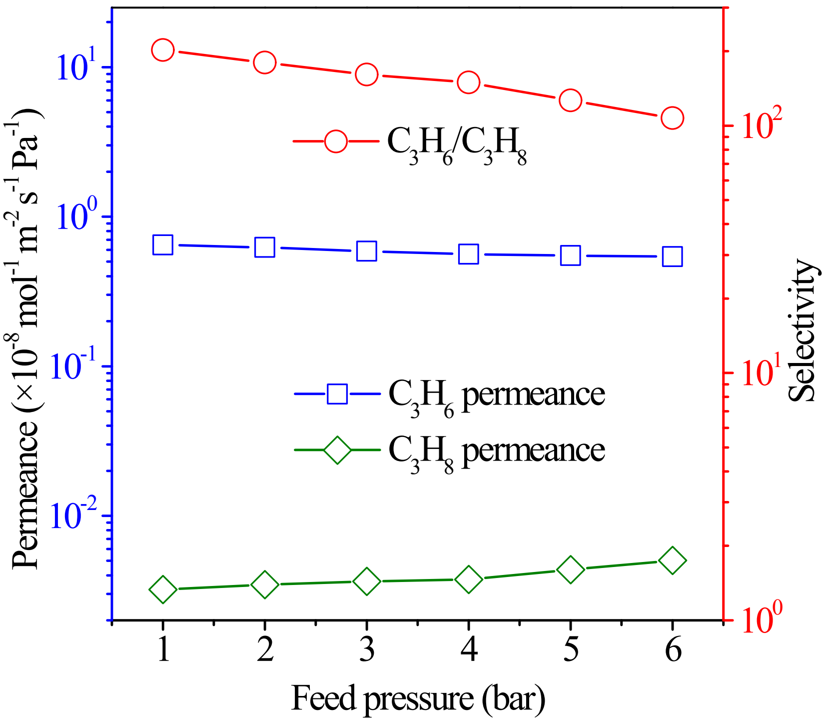

Fig. S22 Effect of feed pressure on separation performance of the ZIF-8 membrane. The membrane was prepared with MeIM/Zn ratio of 4.

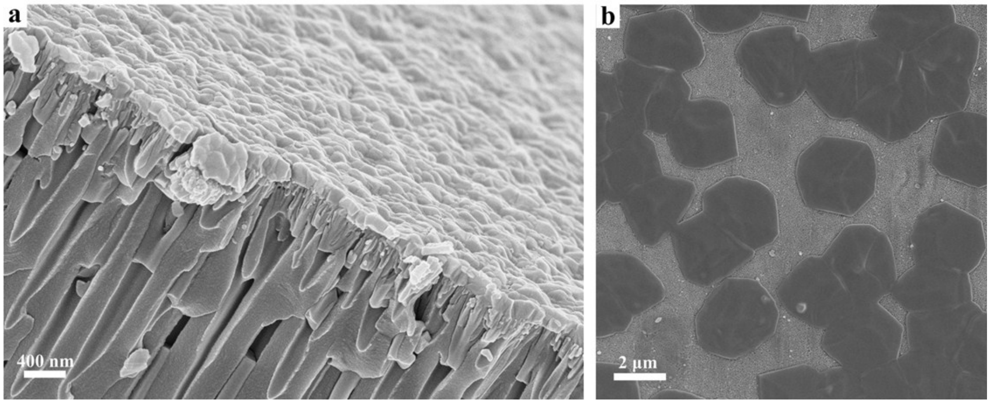

Fig. S23 SEM images of the ZIF-8 membranes prepared with MeIM/Zn ratio of 4 but lower concentration of (a) 0.50 and (b) 0.25 times of the mainly used one.

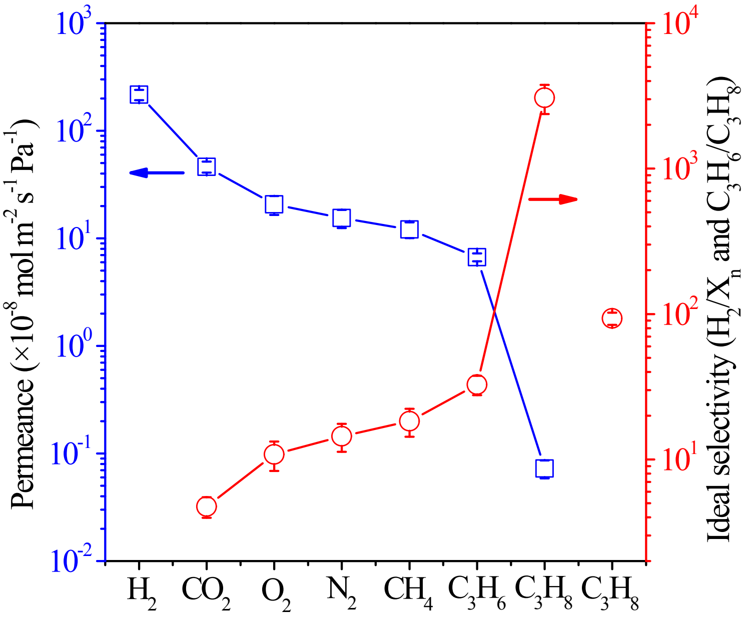

Fig. S24 Single-component permeation of the ultrathin ZIF-8 membrane. The membrane was prepared with MeIM/Zn ratio of 4 but lower concentration of 0.5 times of the mainly used one. Compared to the micrometer-sized membrane prepared in this study, the ultrathin membrane exhibited lower ideal selectivities but higher permeances.

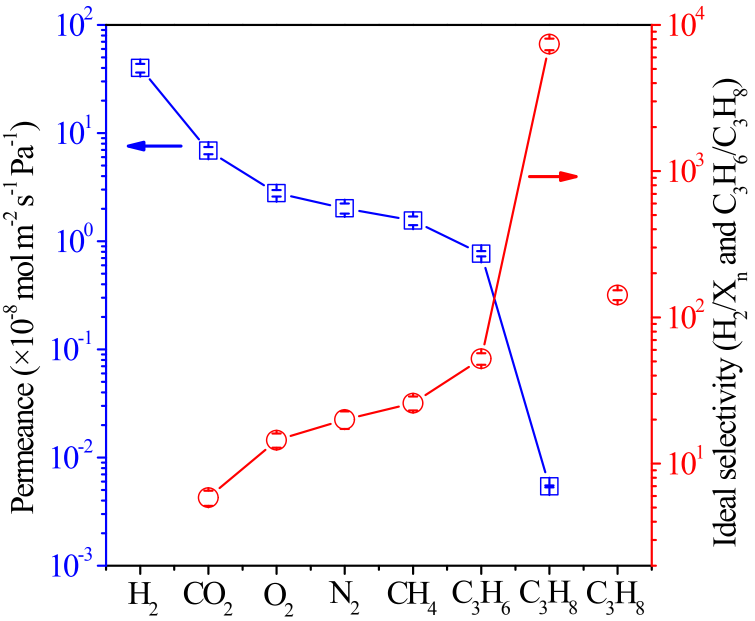

Fig. S25 Single-component permeation of the ZIF-8 hollow fiber membrane. The single-component permeances and ideal selectivities of various gases through the ZIF-8 hollow fiber membrane. The membrane was prepared with MeIM/Zn ratio of 4. The hollow fiber membrane exhibited similar ideal selectivities and permeances as the micrometer-sized membrane prepared in this study.

Table S1 Surface area of the ZIF-8 membrane with various MeIM/Zn ratios.

MeIM/Zn ratios	Content %	Micropore area $m^2 g^{-1}$	ZIF-8 micropore area $m^2 g^{-1}$
2	11.8	13.8	116.4
3	8.2	70.4	854.4
4	7.3	150.9	2056
6	6.2	73.6	1183
8	3.7	47.7	1293
12	3.5	41.4	1175

Table S2 Separation performance of the ZIF-8 membranes prepared by sol-gel transformation. The similar permeances (Per) and selectivities (Sel) of each kind of ZIF-8 membrane indicated the good reproducibility of the proposed sol-gel synthesis. The micrometer-sized ZIF-8 membrane was synthesized with MeIM/Zn ratio of 4. The ultrathin ZIF-8 membrane was fabricated as the micrometer-sized ZIF-8 membrane but with 0.5 times of gel concentration. The ZIF-8 hollow fiber membrane prepared as the micrometer-sized ZIF-8 membrane but with hollow fiber substrate.

Membrane		H_2/CH_4		H_2/C_3H_8		C_3H_6/C_3H_8	
		Per	Sel	Per	Sel	Per	Sel
Micrometer-sized ZIF-8 membrane	M1	25.2	32.3	24.4	7691	0.59	197
	M2	27.9	31.4	26.6	9999	0.58	174
	M3	30.5	27.2	28.5	8332	0.64	203
Thin ZIF-8 membrane	M1	187.5	15.6	188.7	3029	6.32	102
	M2	231.1	24.6	225.0	3845	6.04	115
	M3	190.0	23.3	190.7	3570	5.79	128
ZIF-8 hollow fiber membrane	M1	36.3	26.6	33.4	7406	0.80	187
	M2	41.7	31.1	39.1	9090	0.76	151
	M3	35.5	28.2	33.8	8695	0.71	173

Table S3 Separation performance and synthesis methods of some previously reported high-performance carbon and MOF membranes for H_2/C_3H_8 and C_3H_6/C_3H_8 systems. The values marked by [a] were tested by single-component permeation. YSZ-yttria-stabilized zirconia, PTSC-poly-thiosemicarbazide and BPPO-bromomethylated poly(2,6-dimethyl-1,4-phenylene oxide).

Membrane	Substrate	Synthesis method	C_3H_6/C_3H_8		H_2/C_3H_8		Ref
			Per	Sel	Per	Sel	
Carbon	Al_2O_3 disc	Pyrolysis	0.75	16			1
Carbon	Al_2O_3 disc	Pyrolysis	0.87	17			1
Carbon	Al_2O_3 disc	Pyrolysis	1.4	23			1
ZIF-8	YSZ fiber	Hydrothermal			71	474	2
ZIF-8	Al_2O_3 disc	Hydrothermal	2.1	45			3
ZIF-8	Al_2O_3 disc	Hydrothermal	1.1	30.1			4
ZIF-8	AAO	ENACT-Hydrothermal	9.9[a]	31.6[a]	830[a]	2655[a]	5
ZIF-8	Al_2O_3 disc	Solvothermal	0.2	8			6
ZIF-8	Al_2O_3 disc	Solvothermal	0.34	13.6	18	713	7
ZIF-8/GO	Al_2O_3 disc	Solvothermal			11.9	3816	8
ZIF-8	Al_2O_3 fiber	Cycling	0.4	14.6			9
ZIF-8	Al_2O_3 disc	Layer by layer	0.06	3.5	1.9[a]	60[a]	10
ZIF-8	Al_2O_3 disc	Contra-diffusion	2.5	55			11
ZIF-8/GO	AAO disc	Contra-diffusion	0.16[a]	12[a]	5.46[a]	405[a]	12

ZIF-8/GO	AAO disc	Contra-diffusion	1.7[a]	35[a]	117.6[a]	2409[a]	13
ZIF-8	BPPO flat	Contra-diffusion	0.75[a]	27.8[a]	61[a]	2259[a]	14
ZIF-8	PTSC flat	Contra-diffusion	0.57[a]	150[a]	32[a]	8358[a]	15
ZIF-8	Torlon fiber	Interfacial synthesis	1.2	12	55	370	16
ZIF-8	Torlon fiber	Interfacial synthesis	2.2	65	76	2000	17
ZIF-8	Torlon fiber	Interfacial synthesis	1.5	180	56	3200	18
ZIF-8	PVDF fiber	Vapor-deposition	27	73.4	1178	3126	19
CuBTC	PSF flat	Layer by layer	-	-	7.9[a]	5.7[a]	20
ZIF-90	Al_2O_3 disc	Solvothermal	-	-	27.8	458	21
ZIF-8/ZIF-67	Al_2O_3 disc	Heteroepitaxial growth	3.7	209	-	-	22
ZIF-8/ZIF-67	Al_2O_3 disc	Layer by layer	-	-	1.6	54.7	23
ZIF-90/ZIF-8	Al_2O_3 disc	Contra-diffusion	7.8	40	-	-	24
ZIF-8-67	Al_2O_3 disc	Solvothermal	0.9	50.5	-	-	25
ZIF-8-67	Al_2O_3 disc	Solvothermal	2.0	120	-	-	26

References

1. X. Ma, Y. S. Lin, X. Wei and J. Kniep, *AIChE J.*, 2016, **62**, 491–499.
2. Y. Pan, B. Wang and Z. Lai, *J. Membr. Sci.*, 2012, **421-422**, 292–298.
3. Y. Pan, T. Li, G. Lestari and Z. Lai, *J. Membr. Sci.*, 2012, **390-391**, 93–98.
4. D. Liu, X. Ma, H. Xi and Y. S. Lin, *J. Membr. Sci.*, 2014, **451**, 85–93.
5. G. He, M. Dakhchoune, J. Zhao, S. Huang and K. V. Agrawal, *Adv. Funct. Mater.*, 2018, **28**, 1707427.
6. A. Knebel, B. Geppert, K. Volgmann, D. I. Kolokolov, A. G. Stepanov, J. Twiefel, P. Heitjans, D. Volkmer, and J. Caro, *Science*, 2017, **358**, 347–351.
7. Q. Liu, N. Wang, J. Caro and A. Huang, *J. Am. Chem. Soc.*, 2013, **135**, 17679−17682.
8. A. Huang, Q. Liu, N. Wang, Y. Zhu and J. Caro, *J. Am. Chem. Soc.*, 2014, **136**, 14686–14689.
9. K. Huang, Z. Y. Dong, Q. Q. Li and W. Q. Jin, *Chem. Commun.,* 2013, **49**, 10326–10328.
10. O. Shekhah, R. Swaidan, Y. Belmabkhout, M. Plessis, T. Jacobs, L. J. Barbour, I. Pinnau and M. Eddaoudi, *Chem. Commun.*, 2014, **50**, 2089–2092.
11. H. T. Kwon and H. K. Jeong, *J. Am. Chem. Soc.*, 2013, **135**, 10763–10768.
12. Y. Hu, J. Wei, Y. Liang, H. Zhang, X. Zhang, W. Shen and H. Wang, *Angew. Chem. Int. Ed.*, 2016, **55**, 2048–2052.
13. Y. Hu, Y. Wu, C. Devendran, J. Wei, Y. Liang, M. Matsukata, W. Shen, A. Neild, H. Huang and H. Wang, *J. Mater. Chem. A*, 2017, **5**, 16255–16262.
14. E. Shamsaei, X. Lin, Z. X. Low, Z. Abbasi, Y. Hu, J. Z. Liu and H. Wang, *ACS Appl. Mater. Interfaces,* 2016, **8**, 6236–6244.
15. E. Barankova, X. Tan, L. F. Villalobos, E. Litwiller and K. V. Peinemann, *Angew. Chem. Int.*

Ed., 2017, **56**, 2965–2968.

16. A. J. Brown, N. A. Brunelli, K. Eum, F. Rashidi, J. R. Johnson, W. J. Koros, C. W. Jones and S. Nair, *Science*, 2014, **345**, 72–75.
17. K. Eum, A. Rownaghi, D. Choi, R. R. Bhave, C. W. Jones and S. Nair, *Adv. Funct. Mater.*, 2016, **26**, 5011–5018.
18. K. Eum, C. Ma, A. Rownaghi, C. W. Jones and S. Nair, *ACS Appl. Mater. Interfaces*, 2016, **8**, 25337–25342.
19. W. Li, P. Su, Z. Li, Z. Xu, F. Wang, H. Ou, J. Zhang, G. Zhang and E. Zeng, *Nat. Commun.*, 2017, **8**, 406.
20. D. Nagaraju, D. G. Bhagat, R. Banerjee and U. K. Kharul, *J. Mater. Chem. A*, 2013, **1**, 8828–8835.
21. A. Huang, N. Wang, C. Kong and J. Caro, *Angew. Chem. Int. Ed.,* 2012, **51**, 10551–10555.
22. H. T. Kwon, H. K. Jeong, A. S. Lee, H. S. An and J. S. Lee, *J. Am. Chem. Soc.*, 2015, **137**, 12304–12311.
23. A. Knebel, P. Wulfert-Holzmann, S. Friebe, J. Pavel, I. Strauß, A. Mundstock, F. Steinbach and J. Caro, *Chem. Eur. J.*, 2018, **24**, 5728–5733.
24. M. J. Lee, H. T. Kwon and H. K. Jeong, *Angew. Chem. Int. Ed.*, 2018, **57**, 156–161.
25. C. Wang, F. Yang, L. Sheng, J. Yu, K. Yao, L. Zhang and Y. Pan, *Chem. Commun.*, 2016, **52**, 12578‒12581.
26. F. Hillman, J. M. Zimmerman, S. M. Paek, M. R. A. Hamid, W. T. Lim and H. K. Jeong, *J. Mater. Chem. A*, 2017, **5**, 6090‒6099.